



Fermi-Pasta-Ulam-Tsingou recurrence and cascading mechanism for resonant three-wave interactions

H. M. Yin ^{*} and K. W. Chow 

Department of Mechanical Engineering, University of Hong Kong, Pokfulam, Hong Kong



(Received 22 July 2022; revised 6 March 2023; accepted 26 May 2023; published 29 June 2023)

Evolution of resonant three-wave interaction is governed by quadratic nonlinearities. While propagating localized modes and inverse scattering mechanisms have been studied, transient states such as rogue waves and breathers are not fully understood. Modulation instability modes can trigger growth of disturbances and the eventual development of breathers. Here we study computationally the dynamics beyond the first formation of breathers, and demonstrate repeating patterns of breathers as a manifestation of the Fermi-Pasta-Ulam-Tsingou recurrence (FPUT). While nonlinearity governs the actual dynamics, the range of wave numbers for modulation instability remains a useful indicator. Depending on the stability characteristics of the fundamental mode and the higher-order harmonics (“sidebands”), “regular” and “staggered” FPUT patterns can arise. A “cascading mechanism” provides analytical verification, as the fundamental and sideband modes attain the same magnitude at one particular instant, signifying the first occurrence of a breather. A triangular spectrum is also computed, similar to experimental observations of optical pulses. Such spectra can elucidate the spreading of energy among the sidebands and components of the triad resonance. The concept of “effective energy” is examined and the eigenvalues of the inverse scattering mechanism are computed. Both approaches are utilized to correlate with the occurrence of regular or staggered FPUT. These numerical and analytical studies can enhance our understanding of wave interactions in fluid mechanics and optics.

DOI: [10.1103/PhysRevE.107.064215](https://doi.org/10.1103/PhysRevE.107.064215)

I. INTRODUCTION

Three-wave interactions have been investigated in a wide variety of physical systems, e.g., fluid dynamics, nonlinear optics and plasma physics [1–6]. Resonant interactions occur when the wave numbers and frequencies of the three waves constitute a triad, namely, sum of the wave numbers (frequencies) of two waves being equal to wave number (frequency) of the third wave [7]. Mathematically such three-wave resonant interaction equations are “integrable” [8]. Elegant analytical techniques such as the inverse scattering transform have been applied to derive exact solutions for localized modes and solitons [7–17]. Physically, phenomena linked to such resonance, such as parametric amplification, frequency conversion, and stimulated Raman and Brillouin scattering, have enhanced our understanding of many pattern-forming systems [18–20].

On another important topic in nonlinear dynamics, Fermi-Pasta-Ulam-Tsingou recurrence (FPUT) refers to the tendency of a strongly nonlinear multimodal system to come back to its initial state after potentially complex redistribution of modal energies [21–31]. FPUT was first discovered through the process of energy thermalization in a chain of nonlinear oscillators, subject to the initial excitation of one single or a few normal mode(s) [21]. Energy is first transferred from the initially excited mode to the higher-order modes of the system. In subsequent evolution, energy moves back to the initial state, with the higher-order modes returning to the

ground state with zero excitation [32]. FPUT has been investigated through a huge variety of topics and perspectives, e.g., Bose-Einstein condensates, chains of oscillators, discrete breathers, and heat transport. Our goal here is to investigate these energy exchanges based on the exact, rational and exponential solutions of integrable evolution systems, and in particular, the three-wave resonant interaction equations [15]. A few widely utilized concepts and terminologies relating to solitons and rogue waves will be discussed in the present context first.

The nonlinear Schrödinger equation (NLSE) is a widely adopted model for describing the processes of second-order dispersion and cubic nonlinearity. Many computational and experimental efforts in realizing FPUT are related to nonlinear wave motions in fluid mechanics, magnetic films, and optics [25–27,29,33,34]. In the 1970s, one or two cycles of FPUT could be observed in a wave channel, where slowly varying, hydrodynamic wave packets are governed by the NLSE [25,35]. In the 2000s and 2010s, FPUT was reported for picosecond pulses in association with an optical loop mirror. Modulation instability is believed to play a crucial role [36]. More recently, four or more FPUT cycles could be achieved using an “ultralow loss” fiber. Both “in-phase” and “phase-shifted” patterns could be observed.

From a theoretical perspective, FPUT, localized modes, and breathers have played significant roles since the early days of soliton theory [37–41]. In modern terminologies, simulations and calculations under periodic boundary conditions lead to breathers. For NLSE, breathers periodic in the propagation or transverse variable are known as Kuznetsov-Ma or Akhmediev breathers, respectively [42–44].

^{*}Corresponding author: hmy63110@hku.hk

The issues of nonlinear development of modulation instability and emergence of breathers have been scrutinized intensively. Here we just focus on a “cascading mechanism.” Basically higher-order modes exponentially smaller than the fundamental one initially grow at a higher rate [41]. Eventually all the modes attain roughly the same order of magnitude at one instant in time. The breather is formed; subsequently the breather decays. As the wave profile attains a small amplitude, modulation instability resumes and the cycle is repeated, leading to FPUT [33,45]. This cascading instability of the higher-order modes has been demonstrated for members of the Schrödinger family of evolution equations [43,44,46]. The challenge here is to demonstrate such FPUT dynamics for the three-wave resonant interaction system, where the nonlinearity is quadratic.

The sequence of presentation can now be explained. The constant background solutions for the three-wave resonant interaction system and criteria of modulation instability are derived (Sec. II). We compute the breather solution for this system via the Darboux transformation (Sec. III). If periodic boundary conditions are imposed, sequences of pulsating modes (breathers) arise, decay, and recur for a few cycles before disintegration (Sec. IV). These events are indeed manifestations of FPUT. Regular and staggered patterns of FPUT will be observed. The cascading mechanism will be demonstrated through the first appearance of both types FPUT. The concept of “effective energy” will be elucidated for these FPUT patterns (Sec. V). Eigenvalues of the spatial linear operator are computed, and their properties are consistent with our theoretical framework (Sec. VI). Finally, conclusions are drawn (Sec. VII).

II. BASIC FORMULATIONS

We consider the normalized three-wave resonant interaction equations as [11,15,47]

$$\partial\Psi_1/\partial\tau + V_1\partial\Psi_1/\partial\xi = \Psi_2\Psi_3^*, \quad (1a)$$

$$\partial\Psi_2/\partial\tau + V_2\partial\Psi_2/\partial\xi = -\Psi_1\Psi_3, \quad (1b)$$

$$\begin{aligned} \Psi_1(\xi, \tau) &= \{\delta_1 + w_{11} \exp[i(p\xi + \Omega\tau)] + w_{12} \exp[-i(p\xi + \Omega\tau)]\} \exp[i(K_1\xi + q_1\tau)], \\ \Psi_2(\xi, \tau) &= \{\delta_2 + w_{21} \exp[i(p\xi + \Omega\tau)] + w_{22} \exp[-i(p\xi + \Omega\tau)]\} \exp[i(K_2\xi + q_2\tau)], \\ \Psi_3(\xi, \tau) &= i\{\delta_3 + w_{31} \exp[i(p\xi + \Omega\tau)] + w_{32} \exp[-i(p\xi + \Omega\tau)]\} \times \exp[i[(K_2 - K_1)\xi + (q_2 - q_1)\tau]], \end{aligned} \quad (6)$$

where w_{11} , w_{12} , w_{21} , w_{22} , w_{31} , w_{32} are nonzero real constants; p and Ω represent the wave number and angular frequency of the disturbance, respectively. The criterion for instability is the vanishing of the determinant of the coefficient matrix:

$$\text{Det}(M) = 0, \quad (7a)$$

$$M = \begin{pmatrix} M_1 & 0 & i\delta_3 & 0 & 0 & i\delta_2 \\ 0 & M_2 & 0 & i\delta_3 & i\delta_2 & 0 \\ i\delta_3 & 0 & M_3 & 0 & i\delta_1 & 0 \\ 0 & i\delta_3 & 0 & M_4 & 0 & i\delta_1 \\ 0 & -\delta_2 & -\delta_1 & 0 & M_5 & 0 \\ -\delta_2 & 0 & 0 & -\delta_1 & 0 & M_6 \end{pmatrix}, \quad (7b)$$

$$\begin{aligned} M_1 &= iq_1 + iV_1p + iV_1K_1 + i\Omega, & M_2 &= iq_1 - iV_1p + iV_1K_1 - i\Omega, \\ M_3 &= iq_2 + iV_2p + iV_2K_2 + i\Omega, & M_4 &= iq_2 - iV_2p + iV_2K_2 - i\Omega, \\ M_5 &= q_1 - q_2 - V_3p + V_3K_1 - V_3K_2 - \Omega, & M_6 &= q_1 - q_2 + V_3p + V_3K_1 - V_3K_2 + \Omega. \end{aligned} \quad (7c)$$

$$\partial\Psi_3/\partial\tau + V_3\partial\Psi_3/\partial\xi = \Psi_2\Psi_1^*. \quad (1c)$$

Here ξ and τ are the transverse and propagation directions; V_j , $j = 1, 2, 3$ are the group velocities of the three slowly varying wave packets. By moving in a frame with velocity V_3 , we can for simplicity set V_3 to be zero subsequently.

The three-wave equations [Eqs. (1a)–(1c)] yield plane-wave solutions

$$\begin{aligned} \Psi_1^{[0]}(\xi, \tau) &= \delta_1 \exp[i(K_1\xi + q_1\tau)], \\ \Psi_2^{[0]}(\xi, \tau) &= \delta_2 \exp[i(K_2\xi + q_2\tau)], \\ \Psi_3^{[0]}(\xi, \tau) &= i\delta_3 \exp[i(K_3\xi + q_3\tau)], \end{aligned} \quad (2)$$

where the wave numbers K_j and frequencies q_j satisfy the resonance relations,

$$K_2 = K_1 + K_3, \quad q_2 = q_1 + q_3, \quad (3)$$

and wave-amplitude parameters $(\delta_1, \delta_2, \delta_3)$ satisfy the following conditions:

$$q_1\delta_1 + K_1V_1\delta_1 + \delta_2\delta_3 = 0, \quad (4a)$$

$$q_2\delta_2 + K_2V_2\delta_2 + \delta_1\delta_3 = 0, \quad (4b)$$

$$-\delta_1\delta_2 + (q_1 - q_2)\delta_3 = 0. \quad (4c)$$

The solutions are

$$\begin{aligned} K_1 &= -\frac{q_1^2 - q_1q_2 + \delta_2^2}{(q_1 - q_2)V_1}, & K_2 &= -\frac{-q_1q_2 + q_2^2 - \delta_1^2}{(-q_1 + q_2)V_2}, \\ \delta_3 &= \frac{\delta_1\delta_2}{q_1 - q_2}. \end{aligned} \quad (5)$$

We name the mode (K_2, q_2) as the “parent wave” and the modes (K_1, q_1) , (K_3, q_3) as “daughter waves.” The naming system of parent and daughters is not uniform in the literature.

To investigate the sensitivity to initial conditions, a modulation instability analysis is conducted. While similar tasks have been undertaken in the literature [48], the formulation will be presented here briefly for completeness and for consistency in notation.

Perturbations are introduced on the plane wave [Eq. (2)]:

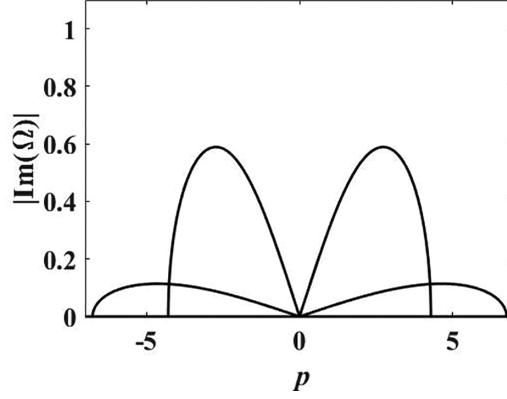


FIG. 1. Modulation instability growth rates $|\text{Im}(\Omega)|$ versus perturbation wave number p with the choice of parameters as $V_1 = 1$, $V_2 = 0.8$, $V_3 = 0$, $\delta_1 = 1$, $\delta_2 = 1$, $q_1 = 2$, and $q_2 = 1$.

The dispersion relation can be expressed as a sixth-power polynomial [Eq. (7a)]. The explicit formulas are tedious, hence we just report the numerical results. Typical instability growth rates are illustrated (Fig. 1).

III. BREATHER MODES

Before we present the computational results on breathers and FPUT patterns, it will be instructive to outline the theoretical scheme to obtain breathers, i.e., modes with periodic boundary conditions in the transverse variable. Equation (1) is integrable. There is a Lax pair formulation,

$$\Phi_\xi = \mathbf{U}\Phi, \quad \Phi_\tau = \mathbf{V}\Phi, \quad (8)$$

where $\Phi(\xi, \tau) = (\phi_1, \phi_2, \phi_3)^T$ is a 3×1 column vector (superscript T = transpose), matrices $\mathbf{U}(\xi, \tau)$ and $\mathbf{V}(\xi, \tau)$ are given by

$$\mathbf{U} = \begin{pmatrix} -\frac{i}{3}(-2V_1 + V_2 + V_3)\lambda & \frac{\Psi_3(\xi, \tau)}{\sqrt{(V_1 - V_3)(V_2 - V_3)}} & -\frac{\Psi_2(\xi, \tau)}{\sqrt{(V_1 - V_2)(V_2 - V_3)}} \\ -\frac{\Psi_3^*(\xi, \tau)}{\sqrt{(V_1 - V_3)(V_2 - V_3)}} & -\frac{i}{3}(V_1 - 2V_2 + V_3)\lambda & \frac{\Psi_1(\xi, \tau)}{\sqrt{(V_1 - V_2)(V_1 - V_3)}} \\ \frac{\Psi_2^*(\xi, \tau)}{\sqrt{(V_1 - V_2)(V_2 - V_3)}} & -\frac{\Psi_1^*(\xi, \tau)}{\sqrt{(V_1 - V_2)(V_1 - V_3)}} & -\frac{i}{3}(V_1 + V_2 - 2V_3)\lambda \end{pmatrix}, \quad (9a)$$

$$\mathbf{V} = \begin{pmatrix} \frac{i}{3}(-V_1 V_2 - V_1 V_3 + 2V_2 V_3)\lambda & -\frac{V_3 \Psi_3(\xi, \tau)}{\sqrt{(V_1 - V_3)(V_2 - V_3)}} & \frac{V_2 \Psi_2(\xi, \tau)}{\sqrt{(V_1 - V_2)(V_2 - V_3)}} \\ \frac{V_3 \Psi_3^*(\xi, \tau)}{\sqrt{(V_1 - V_3)(V_2 - V_3)}} & \frac{i}{3}(-V_1 V_2 + 2V_1 V_3 - V_2 V_3)\lambda & -\frac{V_1 \Psi_1(\xi, \tau)}{\sqrt{(V_1 - V_2)(V_1 - V_3)}} \\ -\frac{V_2 \Psi_2^*(\xi, \tau)}{\sqrt{(V_1 - V_2)(V_2 - V_3)}} & \frac{V_1 \Psi_1^*(\xi, \tau)}{\sqrt{(V_1 - V_2)(V_1 - V_3)}} & \frac{i}{3}(2V_1 V_2 - V_1 V_3 - V_2 V_3)\lambda \end{pmatrix}, \quad (9b)$$

and λ is the complex spectral variable. A constraint on the group velocities, i.e., $V_1 > V_2 > V_3$, should hold. The Darboux transformation for Eq. (1) can be written as [11]

$$\Psi_1^{[1]} = \Psi_1^{[0]} - \frac{i(\lambda^* - \lambda)\sqrt{(V_1 - V_2)(V_1 - V_3)(V_2 - V_3)}\phi_2\phi_3^*}{\phi_1\phi_1^* + \phi_2\phi_2^* + \phi_3\phi_3^*}, \quad (10a)$$

$$\Psi_2^{[1]} = \Psi_2^{[0]} - \frac{i(\lambda^* - \lambda)\sqrt{(V_1 - V_2)(V_2 - V_3)(V_3 - V_1)}\phi_1\phi_3^*}{\phi_1\phi_1^* + \phi_2\phi_2^* + \phi_3\phi_3^*}, \quad (10b)$$

$$\Psi_3^{[1]} = \Psi_3^{[0]} - \frac{i(\lambda^* - \lambda)\sqrt{(V_1 - V_3)(V_2 - V_3)(V_1 - V_2)}\phi_1\phi_2^*}{\phi_1\phi_1^* + \phi_2\phi_2^* + \phi_3\phi_3^*}. \quad (10c)$$

Here the plane-wave states $\Psi_1^{[0]}$, $\Psi_2^{[0]}$, $\Psi_3^{[0]}$ [Eq. (2)] serve as the “seed” solution, and solutions of increasing complexity are built recursively through Eqs. (8)–(10). To obtain the breather modes, we set the transformation

$$\Phi = G\Upsilon, \quad (11)$$

with the 3×3 nonsingular matrix:

$$G = \begin{pmatrix} \exp[i(K_1 x + q_1 t)] & 0 & 0 \\ 0 & \exp[i(K_2 x + q_2 t)] & 0 \\ 0 & 0 & \exp[i(K_1 x + q_1 t) + i(K_2 x + q_2 t)] \end{pmatrix}. \quad (12)$$

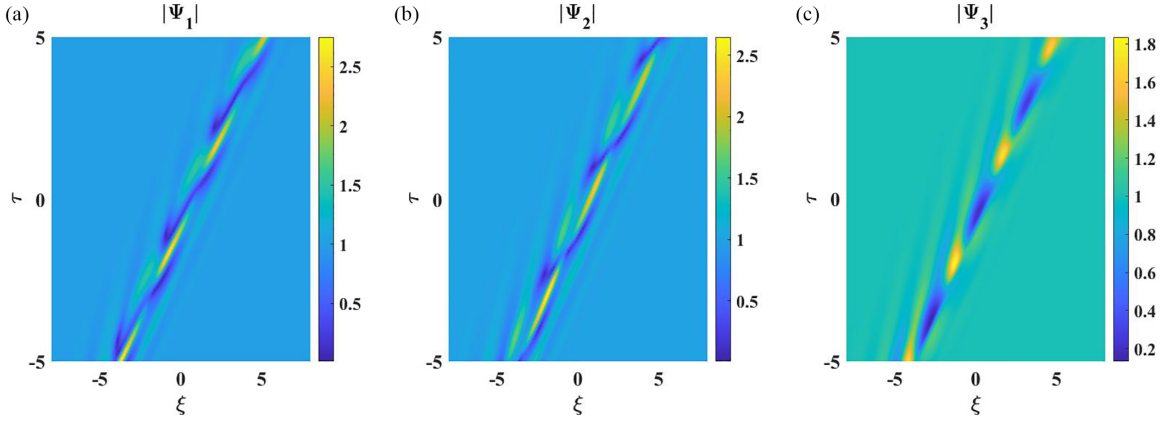


FIG. 2. Fundamental breather of Eq. (1) with the parameters $V_1 = 1$, $V_2 = 0.8$, $V_3 = 0$, $\delta_1 = 1$, $\delta_2 = 1$, $q_1 = 2$, $q_2 = 1$, and $\lambda = 5i$.

Utilizing Eqs. (8) and (11), we derive

$$\Upsilon_\xi = (G^{-1}\mathbf{U}G + G_\xi^{-1}G)\Upsilon = \mathbf{U}_0\Upsilon, \quad (13a)$$

$$\Upsilon_\tau = (G^{-1}\mathbf{V}G + G_\tau^{-1}G)\Upsilon = \mathbf{V}_0\Upsilon, \quad (13b)$$

where

$$\mathbf{U}_0 = \begin{pmatrix} a_{11} & a_{12} & a_{13} \\ a_{21} & a_{22} & a_{23} \\ a_{31} & a_{32} & a_{33} \end{pmatrix}, \quad \mathbf{V}_0 = \begin{pmatrix} b_{11} & b_{12} & b_{13} \\ b_{21} & b_{22} & b_{23} \\ b_{31} & b_{32} & b_{33} \end{pmatrix}. \quad (13c)$$

The elements of the matrices \mathbf{U}_0 , \mathbf{V}_0 are fully listed in Appendix A. Combining Eqs. (11) and (13), the solution for Lax Pair (8) can be obtained as

$$\Phi = \Gamma_1 + \Gamma_2 + \Gamma_3, \quad (14)$$

where $\Gamma_1, \Gamma_2, \Gamma_3$ are expressed in terms of the eigenvalues and eigenvectors of \mathbf{U}_0 . Our approach is different from those in the literature as we include a nonzero wave number in the carrier wave envelope [11]. Typical ‘‘eye-shaped’’ breather modes (a ‘‘peak’’ flanked by two ‘‘valleys’’) can arise (Fig. 2). Similarly, analytical ‘‘four-petal,’’ four-petal, and eye-shaped breathers for the three components have been demonstrated [47] (further descriptions of a four-petal state are given in Sec. IV D). These analytic breather modes will now be compared with the numerically obtained entities. Furthermore, the peaks of the breathers for the Ψ_1 , Ψ_3 components occur at the same spatial-temporal position where the valley of the Ψ_2 component appears. This is different from the coupled NLSE case where the peaks appear at the same place.

IV. FERMI-PASTA-ULAM-TSINGOU RECURRENCE

Instead of localized modes, we now consider wave patterns periodic in the transverse variable. In the fluid mechanics or optics context, this will be the group velocity coordinate or retarded time, respectively. For convenience, we shall take the propagation variable (τ) as ‘‘time’’ in the subsequent discussion. Computationally, periodic boundary conditions are imposed in the numerical simulations. The counterpart

of a localized rogue wave is then a periodic ‘‘breather.’’ A linear calculation such as modulation instability once again proves to be a remarkably accurate and informative indicator of the nonlinear dynamics of the system. More precisely, if the wave number of the disturbance and its higher harmonic belong to the unstable band, two or more classes of breathers may appear. If only the disturbance itself is unstable, only one pattern of a definite wavelength will be observed.

Indeed similar scenarios have occurred in earlier studies, e.g., hydrodynamic surface wave packets governed by the nonlinear Schrödinger equation [35]. The identical principle holds for resonance between long and short waves, e.g., surface and internal modes, where the group velocity of the short wave matches the phase speed of the long wave [49].

In the literature of nonlinear dynamics and the Schrödinger equation, the distinction between Akhmediev breathers (periodic in the transverse variable) and Kuznetsov-Ma breathers (periodic in the propagation variable) is often made. The governing equations for triad resonance here are different [Eq. (1)]. Furthermore, breathers periodic in time or space have not been studied in depth yet. Hence we shall just investigate here the properties of one particular class of breathers with the help of FPUT.

We study the situation where all three plane waves are perturbed by just one selected mode. Analytically we choose, as initial conditions,

$$\begin{aligned} \Psi_1(\xi, 0) &= \delta_1[a_0 + \varepsilon_1 \exp(ip_1\xi) + \varepsilon_1 \exp(-ip_1\xi)] \\ &\quad \times \exp[i(K_1\xi)], \\ \Psi_2(\xi, 0) &= \delta_2[b_0 + \varepsilon_2 \exp(ip_1\xi) + \varepsilon_2 \exp(-ip_1\xi)] \\ &\quad \times \exp[i(K_2\xi)], \\ \Psi_3(\xi, 0) &= i\delta_3[c_0 + \varepsilon_3 \exp(ip_1\xi) + \varepsilon_3 \exp(-ip_1\xi)] \\ &\quad \times \exp[i[(K_2 - K_1)\xi]], \end{aligned} \quad (15)$$

where p_1 is the wave number of the perturbation, $a_0 = \sqrt{1 - \varepsilon_1^2}$, $b_0 = \sqrt{1 - \varepsilon_2^2}$, and $c_0 = \sqrt{1 - \varepsilon_3^2}$, with ε_1 , ε_2 , and ε_3 denoting the (small) amplitude of the disturbance. Computationally a split-step Fourier scheme is implemented. The linear part is solved by Fourier spectral collocation with a

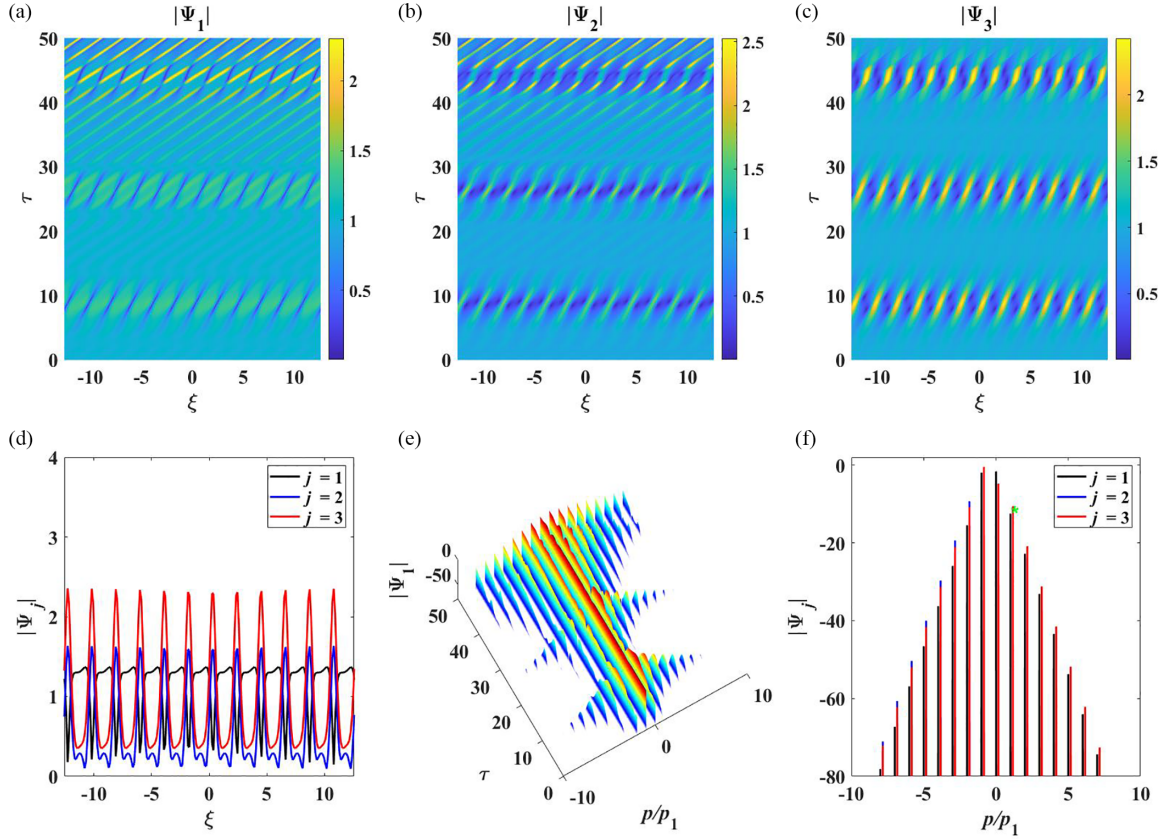


FIG. 3. Regular FPUT: (a)–(c) Numerical simulations for $|\Psi_j|$, $j = 1, 2, 3$ with Eq. (15) as the initial pulse; (d) profiles of breathers at $\tau \approx 8.636$; (e) spectrum of $|\Psi_1|$ versus time τ ; (f) wave amplitude versus normalized wave number at $\tau \approx 8.636$. Parameters chosen are $V_1 = 1$, $V_2 = 0.8$, $V_3 = 0$, $p_1 = 3$, $\delta_1 = 1$, $\delta_2 = 1$, $q_1 = 2$, $q_2 = 1$, $\varepsilon_1 = 0.01$, $\varepsilon_2 = 0.01$, and $\varepsilon_3 = 0.01$.

periodic boundary conditions in the domain $[-L/2, L/2]$. The nonlinear portion is treated by a fourth-order Runge-Kutta method. To ensure the stability of the numerical integrator, we choose the discretization parameter $\Delta\xi = 0.0307$ and a time step $\Delta\tau = 5 \times 10^{-4}$. The evolution pattern for different values of p_1 will be described.

If the wave numbers of the higher harmonics of the perturbation fall outside the modulation instability spectrum, there will only be one preferred wavelength in the FPUT. This will be termed “regular FPUT” in the present discussion. If there are two or more linearly unstable modes, FPUT will exhibit multiple patterns and the name “staggered FPUT” will be adopted.

A. Regular FPUT

As an illustrative example, we consider $p_1 = 3$ in the unstable range. A wave number of $2p_1$ or 6 is in the stable regime. Hence only one breather with wavelength $2\pi/3$ in ξ is observed, appearing at time $\tau \approx 9, 28$, and a few more cycles (Fig. 3). The present FPUT configuration is a doubly periodic pattern in both time (τ) as well as the spatial coordinate (ξ), as illustrated in Figs. 3(a)–3(c), and Fig. 3(d), respectively. The FPUT patterns cannot persist forever and will break up after a few cycles. As FPUT is a periodic pattern in both the ξ and τ directions, the parent wave and daughter waves can be expanded in a Fourier series:

$$\Psi_1(\xi, \tau) = \delta_1 \left[B_0(\tau) + \sum_{j=1}^{\infty} B_{\pm j}(\tau) \exp(\pm i j p_1 \xi) \right] \exp(i K_1 \xi), \quad (16a)$$

$$\Psi_2(\xi, \tau) = \delta_2 \left[C_0(\tau) + \sum_{j=1}^{\infty} C_{\pm j}(\tau) \exp(\pm i j p_1 \xi) \right] \exp(i K_2 \xi), \quad (16b)$$

$$\Psi_3(\xi, \tau) = i \delta_3 \left[D_0(\tau) + \sum_{j=1}^{\infty} D_{\pm j}(\tau) \exp(\pm i j p_1 \xi) \right] \exp[i(K_2 - K_1)\xi], \quad (16c)$$

where B_0, C_0, D_0 are the ‘‘pumps’’ (background plane waves or average values); $B_{\pm j}, C_{\pm j}, D_{\pm j}, j = 1, 2, \dots$ denote the j th harmonic (or sideband) components.

The evolution of the spectrum of $|\Psi_1|$ versus τ is displayed [Fig. 3(e)]. The spectrum is almost symmetric on two sides of the pump. This situation is similar to that in the nonlinear Schrödinger case [50]. Furthermore, FPUT is generated and also sustained by modulation instability. The energy is initially confined to the pump and the first harmonic (spectral plot at $\tau = 0$), but is then transferred to the higher harmonics on each side of the pump [Fig. 3(f)]. A triangular spectrum can be observed in a plot of amplitude versus wave number [Fig. 3(f), $\tau \approx 8.636$]. The (green) star in Fig. 3(f) indicates a normalized wave number of $|\Psi_1|$ being unity. The corresponding wave numbers for $|\Psi_2|$ and $|\Psi_3|$ satisfying the triad condition are then of values different from integers. The spectra of $|\Psi_2|$ and $|\Psi_3|$ are nearly identical. Initially ($\tau = 0$), the energy resides in the pump only. Energy starts to distribute to the harmonics during the stage of modulation instability. At the formation of the breather, the transfer reaches the climax point and the energy of the pump attains a minimum at that time instant. Numerically, at $\tau \approx 8.636$, 80% of the energy remains in the pump component of Ψ_1 . In a bigger contrast, 36% and 58% of energy remain in the pump component of Ψ_2 and Ψ_3 , respectively. The parent component of the triad (Ψ_2) contributes more in the energy sharing during the FPUT cycle. A similar picture holds for the next occurrence of the breather at $\tau \approx 17.976$.

B. Staggered FPUT

For a smaller perturbation wave number, say, $p_1 = 3/2$, both the p_1 and $2p_1 (= 3)$ modes belong to the unstable band. Hence two kinds of breathers, with spatial wavelengths (in ξ) of $4\pi/3$ and $2\pi/3$, appear at $\tau \approx 10.021$ and 17.866 , respectively [Figs. 4(a)–4(f)]. The spectral plot is also illuminating [Fig. 4(g)]. Similar to the FPUT dynamics described in Sec. IV A above, the spectrum is almost symmetric at each side of the pump. For any particular instant in time, there is one dominant wave number and smaller sidebands. As time evolves, the energy flows from the central wave number to the sidebands. The central component then diminishes in strength, but subsequently energy goes back to the central wave number. This pattern will repeat in the propagation variable (τ here) until FPUT breaks up. There is a triangular spectrum, as a plot of the wave amplitude versus the normalized wave number displays this geometric shape [Fig. 4(h)]. Similar to the previous analysis, we employ a (green) star in the spectrum of $|\Psi_1|$ to denote the point of normalized wave number being unity. For the energy transfer, we again confirm that the energy of the central wave number will be smallest at the formation of the breather, as maximum ‘‘thermalization’’ of energy occurs at that point. Numerically, the central wave numbers of Ψ_1, Ψ_2 , and Ψ_3 components at $\tau \approx 10.021$ have 73%, 39%, and 18% of the energy left, respectively. This time the Ψ_3 component contributes most of the energy. At the occurrence of the second type of breather ($\tau \approx 17.866$), the energy levels of the three components are only of 82%, 39%, and 56% of the original values, respectively. The parent component, i.e., Ψ_2 , contributes more energy at this time instant. The scenario

of thermalization of energy is not completely identical to the regular FPUT case of Sec. IV A.

C. Cascading mechanism

For the nonlinear Schrödinger family of evolution equations, modulation instability and a cascading mechanism are often present [43,46]. Higher-order harmonics, exponentially small, initially will nevertheless grow at a rate higher than that of the fundamental mode. All modes eventually reach the same magnitude at roughly the same instant in time (or the value of the propagation variable). A breather is formed. The theoretical calculations consist of perturbation methods and linearization around the higher-order modes. As such calculations have been performed for the derivative and coherently coupled Schrödinger equations [44,46], the treatment here will be brief and full details are explained in Appendix B.

If we assume that the j th harmonic of the parent wave, C_j , goes like an exponential,

$$C_j = v_j \exp[j\Lambda\tau], \quad v_j = \text{initial amplitude}, \quad \Lambda = \text{growth rate},$$

the formation time of the breather can be obtained by simple algebraic manipulation and is given by [Eq. (B21), Appendix B]

$$C_j(\tau) = \exp[j\Lambda(\tau - \tau_j)], \quad \tau_j = -\frac{\ln(v_j)}{j\Lambda}. \quad (17)$$

The precise expressions of $v_j, j = 1, 2, 3, 4$ are tabulated in Appendix B.

We now define an analytical spectrum function F_j as

$$F_j = \ln[C_j(\tau)] = j\Lambda(\tau - \tau_j), \quad j = 1, 2, 3, \dots \quad (18)$$

For the purpose of verifying this cascading mechanism, i.e., Eqs. (17) and (18), we plot the analytical spectra for the regular FPUT case [Fig. 5(a)]. The growth rate Λ is about 0.57. These spectra of sidebands (or harmonics) intersect at one point, $\tau \approx 8.64$, which is consistent with the first appearance of the breather in Fig. 3. For the staggered FPUT case (Fig. 4), the analytical spectra of the first-, second-, third-, and fourth-order sidebands intersect at one point [$\tau \approx 10.02$ in Fig. 5(b)], which is also consistent with the first appearance of the breather in Fig. 4.

We can also obtain Fourier spectra information directly from the numerical simulations. For this purpose, the ‘‘numerical spectrum’’ can be computed by

$$Q_j(\tau) = \frac{1}{L} \int_{-L/2}^{L/2} \Psi_n(\xi, \tau) \exp(-ip_1\xi) d\xi, \quad j = 1, 2, 3, \quad (19)$$

where L denotes the magnitude of the periodic domain, p_1 represents the perturbation wave number. The first harmonic of the Ψ_2 component (parent wave) decreases while those for the Ψ_1 and Ψ_3 components (daughter waves) increase, which implies an energy transfer among the three components of the three-wave resonance. The amplification rate from modulation instability with $p_1 = 3/2$ is about 0.446; i.e.,

$$F_1 = 0.4462(\tau - 10.02). \quad (20)$$

The diamond line in Fig. 5(c) is a graphical plot of Eq. (20). The first-order analytical and numerical spectra

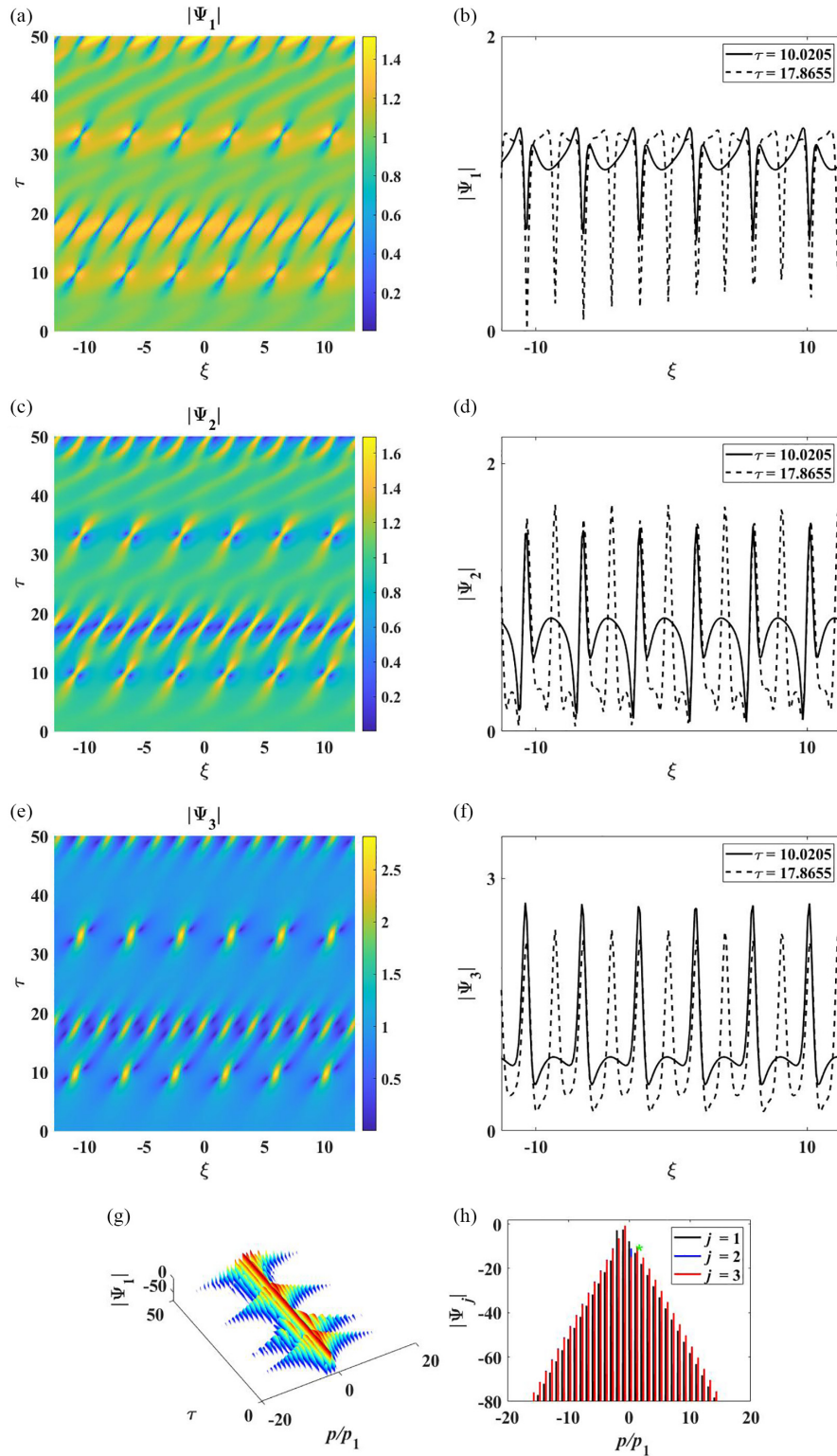


FIG. 4. Staggered FPUT: (a),(c),(e) numerical simulations for $|\Psi_j|$, $j = 1, 2, 3$ with Eq. (15) as the initial pulse; (b),(d),(f) profiles of breathers at $\tau \approx 10.021$ (solid) and 17.866 (dashed); (g) spectrum of $|\Psi_1|$ versus time; (h) wave amplitude versus normalized wave number at $\tau \approx 10.021$. Parameters chosen are $V_1 = 1$, $V_2 = 0.8$, $V_3 = 0$, $p_1 = 1.5$, $\delta_1 = 1$, $\delta_2 = 1$, $q_1 = 2$, $q_2 = 1$, $\varepsilon_1 = 0.01$, $\varepsilon_2 = 0.01$, and $\varepsilon_3 = 0.01$.

agree well. On the other hand, the growth rates of the three components change during the propagation. This situation occurs as the second harmonic is unstable when $p_1 = 3/2$.

D. Comparison between numerical and analytical breathers

For hydrodynamic waves in shallow water and fluid of intermediate depth, the periodic wave actually consists of an infinite array of identical, equally spaced solitons (but moving

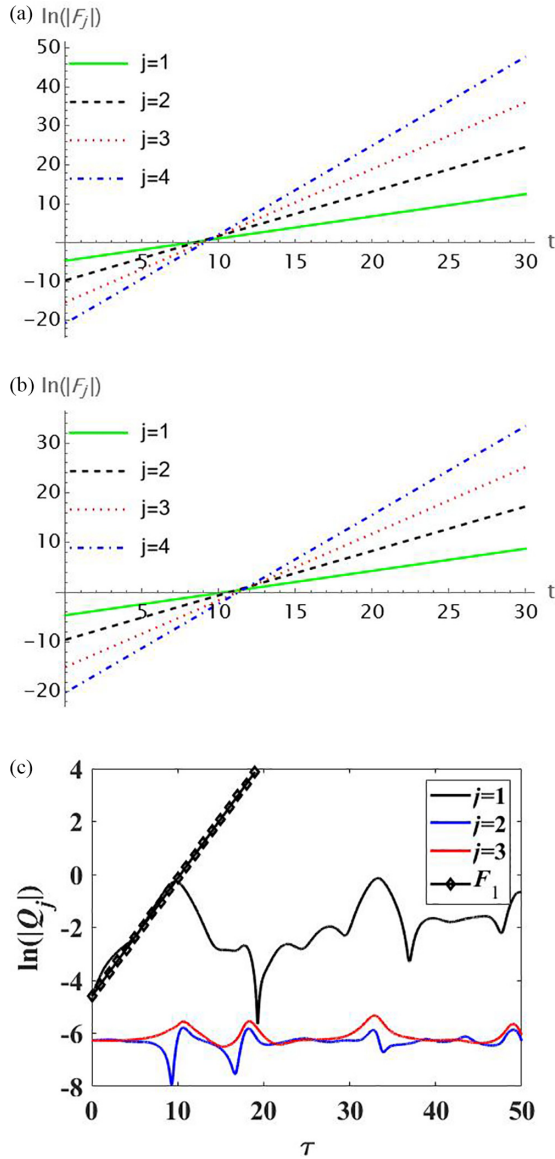


FIG. 5. (a) Analytical spectra of the first-, second-, and third-order sidebands with parameters $V_1 = 1, V_2 = 0.8, V_3 = 0, \delta_1 = 1, \delta_2 = 1, q_1 = 2, q_2 = 1, u_1 = 0.01, v_1 = 0.01, w_1 = 0.01, \Lambda = 0.57,$ and $p_1 = 3$; (b) analytical spectra of the first-, second-, and third-order sidebands with parameters $V_1 = 1, V_2 = 0.8, V_3 = 0, \delta_1 = 1, \delta_2 = 1, q_1 = 2, q_2 = 1, u_1 = 0.01, v_1 = 0.01, w_1 = 0.01, \Lambda = 0.4462,$ and $p_1 = 3/2$; (c) comparison between numerical and analytical spectra for the first harmonic of $|\Psi_1|, |\Psi_2|,$ and $|\Psi_3|$ in Fig. 4.

at a speed different from that of an isolated soliton) [51,52]. For time transient states such as breathers and rogue waves, it will be intriguing to test if some versions of this superposition principle can still hold. Indeed such ideas have been explored for the widely studied nonlinear Schrödinger equation [53]. For the present case of triad resonance with three components and multiple rogue wave modes, we do not expect such a simple superposition principle to hold. Nevertheless, it is instructive to assess the hypothesis by graphical plots.

For this exercise in comparison of wave profiles, we adopt the names commonly used in the literature. Eye-shaped rogue waves are modes with one peak separating two valleys. Four-

petal rogue waves are modes consisting of two peaks, two valleys and a saddle point in the middle. For a few typical parameters, we indeed observe eye-shaped profiles for the Ψ_2 component [Fig. 2(b)]. Similar configuration holds for the numerical simulations [Fig. 3(b)]. In terms of the actual displacements, the analytical description of a rogue mode of the breather fits reasonably well with the computational one (Fig. 6).

V. EFFECTIVE ENERGY

Modulation stability is known to have a strong connection with the configurations of rogue waves observed [54]. We plan to substantiate this link further here. For this purpose, we select Eq. (15) as the initial condition. Effective energy for each component is defined by [15]

$$E_j = \frac{1}{2} \int (|\Psi_j|^2 - |\Psi_{j0}|^2) d\xi, \quad j = 1, 2, 3, \quad (21)$$

where Ψ_{j0} denotes the plane-wave background and the integration is taken over one period in the transverse variable ξ .

In order to understand the dynamics, we describe a correlation among modulation instability growth rate, group velocity V_1 , and the modulation wave number p (Fig. 7). We first trace the variation of growth rates as V_1 varies, using a typical value $p = 3$ studied earlier (black solid line in Fig. 7). We exclude the neighborhood V_1 being zero, as a singular solution will then occur in Eq. (5). The key features are as follows:

- (i) As V_1 moves from -1 to 0 , the modulation instability growth rate first increases, attains a local maximum, and then decreases. Meanwhile, the instability sideband broadens as V_1 approaches zero.
- (ii) As V_1 moves from 0 to 1 , the same trend holds; i.e., the instability growth rate increases and then decreases as V_1 approaches unity. Again the instability sideband is wider for values of V_1 closer to zero.

The concept of effective energy can now be utilized to investigate the effects of modulation instability. Equation (15) is chosen as the initial condition. We compute the effective energies (E_1, E_2, E_3), and show the results in a contour plot with respect to the group velocity V_1 and propagation variable τ (Fig. 8).

For any fixed value of V_1 , say, $V_1 = -0.8$, one can trace the development of the energy (or in an equivalent manner, the displacement) by moving along a horizontal line for increasing τ . There is an extremum in effective energy at $\tau \approx 6$, corresponding to the formation of a breather. The modes Ψ_1, Ψ_3 (or E_1, E_3) are in phase as they both exhibit positive effective energy at the formation of the breather. The mode Ψ_2 (or E_2) is out of phase with these two as the effective energy is negative.

This concept of effective energy also clearly illustrates the dynamics of different types of breathers. For the case where only the fundamental disturbance is unstable, there is just one type of breather in the FPUT patterns. Indeed the value of the propagation variable for the first occurrence of the breather is half the FPUT period. We can inspect again, say, $V_1 = -0.8$. The breather first arises at $\tau \approx 6$ (rectangle in dotted lines, left plot of Fig. 8) and recurs at $\tau \approx 18$ (rectangle in solid lines), with a period of 12.

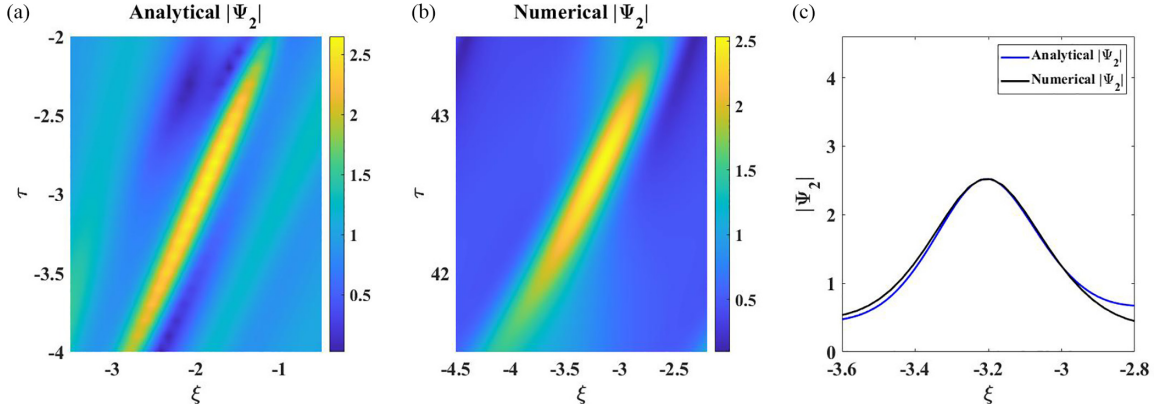


FIG. 6. Zoomed-in view of the region in (a) Fig. 2(b) and (b) Fig. 3(b); (c) comparison of the profiles of the Ψ_2 component from these approaches at a fixed time instant (τ).

For a smaller value of V_1 , say, $V_1 = -0.4$, the modulation instability spectrum is wider (more unstable sidebands), and two or more types of breathers can appear. We can readily confirm this feature by starting at $V_1 = -0.4$ and moving horizontally for increasing τ (rectangle in dashed line, left plot of Fig. 8).

The time for the first formation of the breather will be smaller if the modulation instability is stronger. From the perspective of the cascading mechanism, this is plausible as strong instability will need a smaller time for all the modes to attain roughly the same magnitude [46]. The analytical significance of modulation instability is thus remarkable, as a linear calculation can predict the first formation time of breathers and the types of these pulsating modes, even though strong nonlinearity is affecting a substantial portion of the evolution process. A typical example of FPUT is displayed (Fig. 9).

VI. EIGENVALUES

Formulations of the inverse scattering transform for the three-wave interaction equations have been documented

extensively in the literature [16,48]. Hence we shall concentrate on one aspect relevant to our present discussion, namely, the spectra of eigenvalues of the spatial linear operator. More precisely, the eigenvalues of

$$\begin{bmatrix} \phi_1(\xi, \tau) \\ \phi_2(\xi, \tau) \\ \phi_3(\xi, \tau) \end{bmatrix}_\xi = \mathbf{U} \begin{bmatrix} \phi_1(\xi, \tau) \\ \phi_2(\xi, \tau) \\ \phi_3(\xi, \tau) \end{bmatrix} \quad (22)$$

are independent of τ . This implies that the dynamics of the slowly varying wave packets at any time τ is determined by the spectra of the eigenvalues of the spatial linear operator at the initial condition. Following the analysis from earlier works [55], we assert that these eigenvalues will determine the amplitudes of the nonlinear waves. To associate the latter with FPUT, we compute the spectra of eigenvalues of the spatial linear operator with the initial condition [Eq. (15)]. To this end, the Fourier collocation method is employed. The eigenfunction $\Phi(\xi, \tau) = (\phi_1, \phi_2, \phi_3)^T$ and the initial condition are expanded in a Fourier series in the domain $[-L/2, L/2]$. The matrix eigenvalue problem for the Fourier coefficients is then solved:

$$\phi_1(\xi) = \sum_{n=-N}^N a_{1,n} \exp(ink_0\xi), \quad \phi_2(\xi) = \sum_{n=-N}^N a_{2,n} \exp(ink_0\xi), \quad (23a)$$

$$\phi_3(\xi) = \sum_{n=-N}^N a_{3,n} \exp(ink_0\xi), \quad \Psi_1(\xi, 0) = \sum_{n=-N}^N b_{1,n} \exp(ink_0\xi), \quad (23b)$$

$$\Psi_2(\xi, 0) = \sum_{n=-N}^N b_{2,n} \exp(ink_0\xi), \quad \Psi_3(\xi, 0) = \sum_{n=-N}^N b_{3,n} \exp(ink_0\xi), \quad (23c)$$

where $k_0 = 2\pi/L$. Combining Eqs. (22) and (23) and collecting terms, we obtain the eigenvalue problem for the Fourier coefficients $a_{j,n}$, $b_{j,n}$, $j = 1, 2, 3$. We consider two representative examples. The eigenvalues, λ , for $p_1 = 3$ (red dots) and 1.5 (blue circle), correspond to the regular and staggered FPUT patterns (Fig. 10). From the fine resolution plot

[Fig. 10(b)], we can see that the maximum value of the imaginary part of the eigenvalues for the $p_1 = 3$ case is smaller than that of the $p_1 = 1.5$ case. Following the logic of the previous analysis, the amplitude of the slowly varying wave packet for the cases of $p_1 = 3$ is smaller than that of $p_1 = 1.5$. The former is at a value of about 2.5, while the latter almost

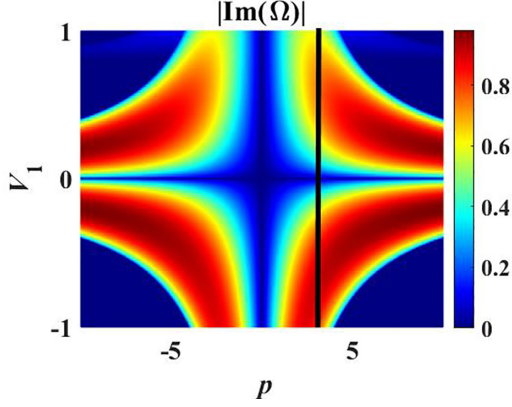


FIG. 7. Contour plot of the modulation instability growth rate with respect to V_1 and p ; black solid line denotes $p = 3$. Parameters are $V_2 = 0.8$, $V_3 = 0$, $\delta_1 = 1$, $\delta_2 = 1$, $q_1 = 2$, and $q_2 = 1$.

reaches 3. From the profiles of the breathers in Figs. 3 and 4, these results are in accordance with those obtained from the analysis of the eigenvalues.

VII. CONCLUSIONS

Three-wave resonant interaction systems are studied, with the group velocities of three waves along the direction of the transverse variable, i.e., V_j , $j = 1, 2, 3$, as parameters. Modulation instability modes play an important role in this dynamical system with quadratic nonlinearities. While the evolution of the wave profile is dictated by nonlinearity, the range of wave numbers necessary for instability still remains a powerful indicator. Indeed under the theoretical framework of periodic boundary conditions, a periodic array of pulsating modes (known as a breather) can occur and will repeat for a few cycles before disintegration. This is connected with the classical phenomenon of FPUT. Depending on the wavelength of the initial disturbance, one, two, or more types will appear.

A fundamental eye-shape breather is established for a resonant triad by utilizing the Darboux transformation method. Theoretically this analytical breather should satisfy the relation $V_1 > V_2 > V_3$. Two types of FPUT, i.e., repeated occurrences of breathers, are constructed numerically. One is a regular pattern, where one dominant wave number from modulation instability triggers the cascading mechanism. The

other is a staggered form, where two (or more) wave numbers from the initial perturbations belong to the unstable band. In terms of computational results, there are two (or more) periods for the recurrence of these staggered FPUT patterns. The cascading mechanism is analyzed to predict the formation time for both regular and staggered FPUT patterns and the growth of the first sideband by Fourier expansion. Triangular spectra versus time and normalized wave number are displayed to elucidate the property of the FPUT. Comparing the initial triangular spectrum with that at the formation time yields the energy transfer among these harmonics of the three components.

We also examine the concept of effective energy. By scrutinizing the variation of the effective energy with the group velocity parameter, we identify the occurrence of different types of breathers, i.e., regular and staggered forms, and the period of FPUT profiles. Finally, to enhance the association with theoretical investigation, a comparison between the analytical and numerical breathers is conducted.

There are still unresolved issues and challenges for future investigations. For example, the second-order rogue waves have been established analytically [48]. However, physical applications and comparisons with experimental data (if any) have not been attempted. It would be instructive to explain or describe the usage of these analytical solutions in physical applications such as fluid mechanics, especially in the context of surface and internal waves. Besides the Darboux transformation and computational schemes, the elegant techniques of “finite gap” integration and the inverse scattering transform have also been employed [56,57]. Physically, the nonlinear stages of modulation instability involve excitation of higher-order modes. Geometrically, a “finite gap” integration scheme for the periodic boundary condition problem of the governing equations will also induce many modes (or “bands”). The prominent band leads to the intensively studied Akhmediev breather, but eventually other bands and breather modes also enter the picture. We believe that a significant amount of knowledge (and surprise) in the fields of FPUT and wave propagation [58,59] will be awaiting for scientists and researchers.

ACKNOWLEDGMENTS

Partial financial support has been provided by the Research Grants Council General Research Fund Contract No. HKU 17204722.

APPENDIX A

The elements of the matrices [Eq. (13c)] are given by

$$a_{11} = -\frac{i}{3} \left[\frac{3(q_1^2 - q_1 q_2 + \delta_2^2)}{(q_1 - q_2)V_1} + (-2V_1 + V_2 + V_3)\lambda \right], \quad (\text{A1})$$

$$a_{12} = a_{21} = \frac{i\delta_1\delta_2}{(q_1 - q_2)\sqrt{(V_1 - V_3)(V_2 - V_3)}}, \quad a_{13} = -a_{31} = -\frac{\delta_2}{\sqrt{(V_1 - V_2)(V_2 - V_3)}}, \quad (\text{A2})$$

$$a_{23} = -a_{32} = \frac{\delta_1}{\sqrt{(V_1 - V_2)(V_1 - V_3)}}, \quad a_{22} = -\frac{i}{3} \left[\frac{3(q_1 q_2 - q_2^2 + \delta_1^2)}{(q_1 - q_2)V_2} + (V_1 - 2V_2 + V_3)\lambda \right], \quad (\text{A3})$$

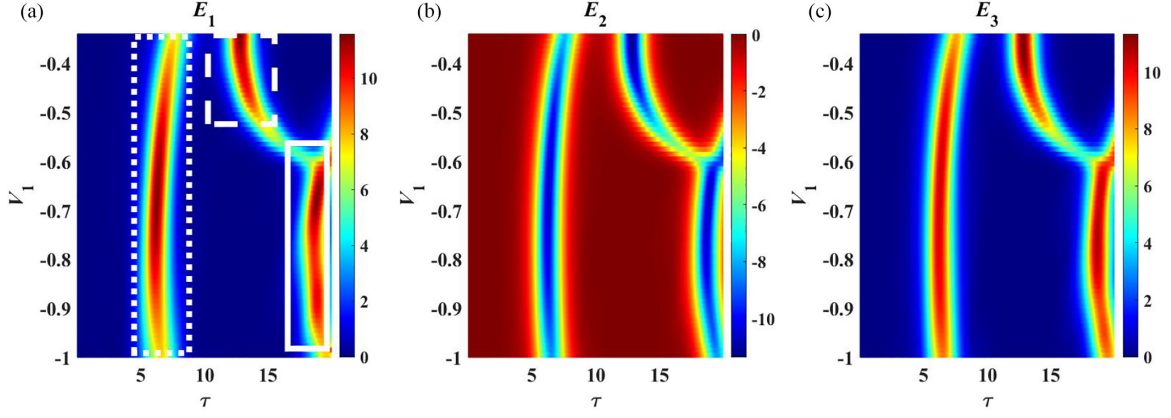


FIG. 8. Contour plot for the evolution of effective energy with τ for various group velocities V_1 . Parameters selected are $V_2 = 0.8$, $V_3 = 0$, $p_1 = 3$, $\delta_1 = 1$, $\delta_2 = 1$, $q_1 = 2$, $q_2 = 1$, $\varepsilon_1 = 0.01$, $\varepsilon_2 = 0.01$, and $\varepsilon_3 = 0.01$.

$$a_{33} = -\frac{i}{3} \left[\frac{3(q_1 q_2 - q_2^2 + \delta_1^2)}{(q_1 - q_2)V_2} + \frac{3(q_1^2 - q_1 q_2 + \delta_2^2)}{(q_1 - q_2)V_1} + (V_1 + V_2 - 2V_3)\lambda \right], \quad (\text{A4})$$

$$b_{11} = \frac{i}{3} [3q_1 + 2V_2 V_3 \lambda - V_1 (V_2 + V_3) \lambda], \quad (\text{A5})$$

$$b_{12} = b_{21} = -\frac{iV_3 \delta_1 \delta_2}{(q_1 - q_2) \sqrt{(V_1 - V_3)(V_2 - V_3)}}, \quad b_{13} = -b_{31} = \frac{V_2 \delta_2}{\sqrt{(V_1 - V_2)(V_2 - V_3)}}, \quad (\text{A6})$$

$$b_{23} = -b_{32} = -\frac{V_1 \delta_1}{\sqrt{(V_1 - V_2)(V_1 - V_3)}}, \quad b_{22} = \frac{i}{3} [3q_2 + 2V_1 V_3 \lambda - V_2 (V_1 + V_3) \lambda], \quad (\text{A7})$$

$$b_{33} = \frac{i}{3} [3q_1 + 3q_2 + 2V_1 V_3 \lambda - V_3 (V_1 + V_2) \lambda]. \quad (\text{A8})$$

APPENDIX B

Cascading instability can be used to study the growth of the sidebands of FPUT [43]. This cascading mechanism for triad resonance is elucidated in precise detail here. For the cascading instability of the second-order sidebands, we truncate Eq. (16) to

$$\Psi_1(\xi, \tau) = \delta_1 \left[\begin{array}{l} B_0(\tau) + B_1(\tau) \exp(ip_1 \xi) + B_{-1}(\tau) \exp(-ip_1 \xi) \\ + B_2(\tau) \exp(2ip_1 \xi) + B_{-2}(\tau) \exp(-2ip_1 \xi) \end{array} \right] \exp(iK_1 \xi), \quad (\text{B1})$$

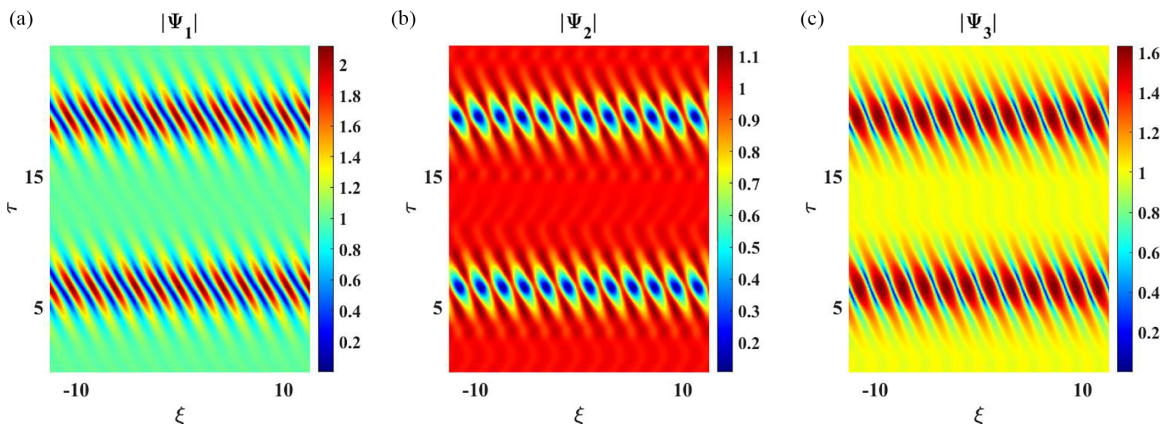


FIG. 9. (a–c) Eye-shaped, dark, and eye-shaped FPUT wave profiles patterns, respectively, with parameters $V_1 = -1$, $V_2 = 0.8$, $V_3 = 0$, $p_1 = 3$, $\delta_1 = 1$, $\delta_2 = 1$, $q_1 = 2$, $q_2 = 1$, $\varepsilon_1 = 0.01$, $\varepsilon_2 = 0.01$, and $\varepsilon_3 = 0.01$.

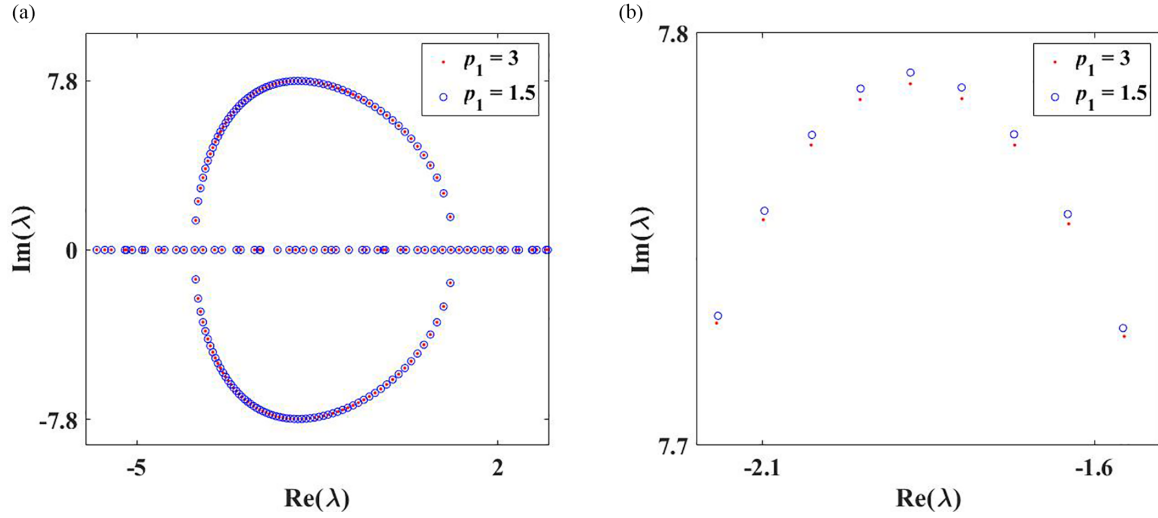


FIG. 10. (a) Eigenvalues of the spatial linear operator [Eq. (22)] with the initial conditions for the two cases of $p_1 = 3$ (red dots) and 1.5 (blue circle); (b) zoomed-in view for one selected region.

$$\Psi_2(\xi, \tau) = \delta_2 \left[\begin{array}{l} C_0(\tau) + C_1(\tau) \exp(ip_1\xi) + C_{-1}(\tau) \exp(-ip_1\xi) \\ + C_2(\tau) \exp(2ip_1\xi) + C_{-2}(\tau) \exp(-2ip_1\xi) \end{array} \right] \exp(iK_2\xi), \quad (\text{B2})$$

$$\Psi_3(\xi, \tau) = i\delta_3 \left[\begin{array}{l} D_0(\tau) + D_1(\tau) \exp(ip_1\xi) + D_{-1}(\tau) \exp(-ip_1\xi) \\ + D_2(\tau) \exp(2ip_1\xi) + D_{-2}(\tau) \exp(-2ip_1\xi) \end{array} \right] \exp[i(K_2 - K_1)\xi]. \quad (\text{B3})$$

On setting

$$B_0(\tau) = \exp(iq_1\tau), \quad C_0(\tau) = \exp(iq_2\tau), \quad D_0(\tau) = \exp[i(q_2 - q_1)\tau], \quad (\text{B4})$$

$$B_{\pm 1}(\tau) = \exp(iq_1\tau)u_1 \exp(\pm\Lambda\tau), \quad C_{\pm 1}(\tau) = \exp(iq_2\tau)v_1 \exp(\pm\Lambda\tau), \quad (\text{B5})$$

$$D_{\pm 1}(\tau) = \exp[i(q_2 - q_1)\tau]w_1 \exp(\pm\Lambda\tau), \quad (\text{B6})$$

and substituting Eqs. (B4)–(B6) into Eq. (1), we have

$$i \exp[i(q_1 - q_2)\tau] \delta_2 \delta_3 C_2(\tau) + \delta_1 B_{2,\tau}(\tau) = 0, \quad (\text{B7})$$

$$iu_1 w_1 \delta_1 \delta_3 \exp(iq_2\tau + 2\Lambda\tau) + \delta_2 C_{2,\tau}(\tau) = 0, \quad (\text{B8})$$

$$-\exp(-iq_1\tau) \delta_1 \delta_2 C_2(\tau) + i\delta_3 D_{2,\tau}(\tau) = 0. \quad (\text{B9})$$

Separating modal dependence as

$$B_2(\tau) = \exp(iq_1\tau)u_2 \exp(2\Lambda\tau), \quad C_2(\tau) = \exp(iq_2\tau)v_2 \exp(2\Lambda\tau), \quad (\text{B10})$$

$$D_2(\tau) = \exp[i(q_2 - q_1)\tau]w_2 \exp(2\Lambda\tau), \quad (\text{B11})$$

we obtain

$$u_2 = \frac{u_1 w_1 \delta_3^2}{(q_1 - 2i\Lambda)(q_2 - 2i\Lambda)}, \quad v_2 = -\frac{u_1 w_1 \delta_1 \delta_3}{q_2 \delta_2 - 2i\delta_2 \Lambda}, \quad w_2 = \frac{u_1 w_1 \delta_1^2}{(q_2 - 2i\Lambda)(-q_1 + q_2 - 2i\Lambda)}. \quad (\text{B12})$$

Similarly, we can get the third- and fourth-order sidebands as

$$B_3(\tau) = \exp(iq_1\tau)u_3 \exp(3\Lambda\tau), \quad C_3(\tau) = \exp(iq_2\tau)v_3 \exp(3\Lambda\tau), \quad (\text{B13})$$

$$D_3(\tau) = \exp[i(q_2 - q_1)\tau]w_3 \exp(3\Lambda\tau), \quad (\text{B14})$$

$$B_4(\tau) = \exp(iq_1\tau)u_4 \exp(4\Lambda\tau), \quad C_4(\tau) = \exp(iq_2\tau)v_3 \exp(4\Lambda\tau), \quad (\text{B15})$$

$$D_4(\tau) = \exp[i(q_2 - q_1)\tau]w_4 \exp(4\Lambda\tau), \quad (\text{B16})$$

where

$$u_3 = \frac{(u_2w_1 + u_1w_2)\delta_3^2}{(q_1 - 3i\Lambda)(q_2 - 3i\Lambda)}, \quad v_3 = -\frac{(u_2w_1 + u_1w_2)\delta_1\delta_3}{\delta_2(q_2 - 3i\Lambda)}, \quad (\text{B17})$$

$$w_3 = \frac{(u_2w_1 + u_1w_2)\delta_1^2}{(q_2 - 3i\Lambda)(-q_1 + q_2 - 3i\Lambda)}, \quad (\text{B18})$$

$$u_4 = \frac{(u_3w_1 + u_2w_2 + u_1w_3)\delta_3^2}{(q_1 - 4i\Lambda)(q_2 - 4i\Lambda)}, \quad v_4 = -\frac{(u_3w_1 + u_2w_2 + u_1w_3)\delta_1\delta_3}{\delta_2(q_2 - 4i\Lambda)}, \quad (\text{B19})$$

$$w_4 = \frac{(u_3w_1 + u_2w_2 + u_1w_3)\delta_1^2}{(q_2 - 4i\Lambda)(-q_1 + q_2 - 4i\Lambda)}. \quad (\text{B20})$$

We can generalize this trend to the j th harmonic as

$$B_j(\tau) \propto u_j \exp(j\Lambda\tau), \quad C_j(\tau) \propto v_j \exp(j\Lambda\tau), \quad D_j(\tau) \propto w_j \exp(j\Lambda\tau). \quad (\text{B21})$$

-
- [1] M. J. Ablowitz and H. Segur, *Solitons and the Inverse Scattering Transform*, (SIAM, Philadelphia, 1981).
- [2] J. L. Hammack and D. Henderson, Resonant interactions among surface water waves, *Annu. Rev. Fluid Mech.* **25**, 55 (1993).
- [3] K. Lamb, Tidally generated near-resonant internal wave triads at a shelf break, *Geophys. Res. Lett.* **34**, L18607 (2007).
- [4] I. Y. Dodin and N. Fisch, Storing, Retrieving, and Processing Optical Information by Raman Backscattering in Plasmas, *Phys. Rev. Lett.* **88**, 165001 (2002).
- [5] F. Baronio, M. Conforti, C. De Angelis, A. Degasperis, M. Andreana, V. Couderc, and A. Barthélemy, Velocity-Locked Solitary Waves in Quadratic Media, *Phys. Rev. Lett.* **104**, 113902 (2010).
- [6] G. Burlak, S. Koshevaya, M. Hayakawa, E. Gutierrez-D, and V. Grimalsky, Acousto-optic solitons in fibers, *Opt. Rev.* **7**, 323 (2000).
- [7] B. Yang and J. Yang, Rogue waves in (2+1)-dimensional three-wave resonant interactions, *Physica D (Amsterdam)* **432**, 133160 (2022).
- [8] V. Zakharov and S. Manakov, The theory of resonance interaction of wave packets in nonlinear media, *Zh. Exp. Teor. Fiz.* **69**, 1654 (1975).
- [9] D. Kaup, A. Reiman, and A. Bers, Space-time evolution of nonlinear three-wave interactions. I. Interaction in a homogeneous medium, *Rev. Mod. Phys.* **51**, 275 (1979).
- [10] A. D. Craik, *Wave Interactions and Fluid Flows* (Cambridge University Press, New York, 1988).
- [11] G. Mu and Z. Qin, High order rational solitons and their dynamics of the 3-wave resonant interaction equation, *Physica D (Amsterdam)* **435**, 133287 (2022).
- [12] X. Wang, J. Cao, and Y. Chen, Higher-order rogue wave solutions of the three-wave resonant interaction equation via the generalized Darboux transformation, *Phys. Scr.* **90**, 105201 (2015).
- [13] S. Chen, F. Baronio, J. Soto-Crespo, P. Grelu, M. Conforti, and S. Wabnitz, Optical rogue waves in parametric three-wave mixing and coherent stimulated scattering, *Phys. Rev. A* **92**, 033847 (2015).
- [14] S. Chen, J. M. Soto-Crespo, and P. Grelu, Watch-hand-like optical rogue waves in three-wave interactions, *Opt. Express* **23**, 349 (2015).
- [15] F. Baronio, M. Conforti, A. Degasperis, and S. Lombardo, Rogue Waves Emerging from the Resonant Interaction of Three Waves, *Phys. Rev. Lett.* **111**, 114101 (2013).
- [16] A. Degasperis and S. Lombardo, Rational solitons of wave resonant-interaction models, *Phys. Rev. E* **88**, 052914 (2013).
- [17] A. Degasperis and S. Lombardo, Exact solutions of the 3-wave resonant interaction equation, *Physica D (Amsterdam)* **214**, 157 (2006).
- [18] E. Ibragimov and A. Struthers, Second-harmonic pulse compression in the soliton regime, *Opt. Lett.* **21**, 1582 (1996).
- [19] M. Conforti, F. Baronio, A. Degasperis, and S. Wabnitz, Parametric frequency conversion of short optical pulses controlled by a cw background, *Opt. Express* **15**, 12246 (2007).
- [20] A. Picozzi and M. Haelterman, Parametric Three-Wave Soliton Generated from Incoherent Light, *Phys. Rev. Lett.* **86**, 2010 (2001).
- [21] E. Fermi, J. Pasta, and S. Ulam, Los Alamos Report LA-1940, 1955, in *Collected Papers of Enrico Fermi* (University of Chicago Press, Chicago, 1965), Vol. 2.
- [22] D. K. Campbell, P. Rosenau, and G. M. Zaslavsky, Introduction: The Fermi–Pasta–Ulam problem—the first fifty years, *Chaos* **15**, 015101 (2005).
- [23] G. Gallavotti, *The Fermi-Pasta-Ulam Problem: A Status Report* (Springer, New York, 2007).
- [24] N. N. Akhmediev, Déjà vu in optics, *Nature (London)* **413**, 267 (2001).
- [25] B. M. Lake, H. C. Yuen, H. Rungaldier, and W. E. Ferguson, Nonlinear deep-water waves: Theory and experiment. Part 2.

- Evolution of a continuous wave train, *J. Fluid Mech.* **83**, 49 (1977).
- [26] N. Akhmediev, D. Heatley, G. Stegeman, and E. Wright, Pseudorecurrence in Two-Dimensional Modulation Instability with a Saturable Self-Focusing Nonlinearity, *Phys. Rev. Lett.* **65**, 1423 (1990).
- [27] S. Trillo, G. Deng, G. Biondini, M. Klein, G. F. Clauss, A. Chabchoub, and M. Onorato, Experimental Observation and Theoretical Description of Multisoliton Fission in Shallow Water, *Phys. Rev. Lett.* **117**, 144102 (2016).
- [28] M. Guasoni, J. Garnier, B. Rumpf, D. Sugny, J. Fatome, F. Amrani, G. Millot, and A. Picozzi, Incoherent Fermi-Pasta-Ulam Recurrences and Unconstrained Thermalization Mediated by Strong Phase Correlations, *Phys. Rev. X* **7**, 011025 (2017).
- [29] D. Pierangeli, M. Flammini, L. Zhang, G. Marcucci, A. Agrat, P. Grinevich, P. Santini, C. Conti, and E. DelRe, Observation of Fermi-Pasta-Ulam-Tsingou Recurrence and Its Exact Dynamics, *Phys. Rev. X* **8**, 041017 (2018).
- [30] S.-C. Chen, C. Liu, X. Yao, L.-C. Zhao, and N. Akhmediev, Extreme spectral asymmetry of Akhmediev breathers and Fermi-Pasta-Ulam recurrence in a Manakov system, *Phys. Rev. E* **104**, 024215 (2021).
- [31] G. Vanderhaegen, P. Szriftgiser, A. Kudlinski, M. Conforti, S. Trillo, M. Droques, and A. Mussot, Observation of four Fermi-Pasta-Ulam-Tsingou recurrences in an ultra-low-loss optical fiber, *Opt. Express* **28**, 17773 (2020).
- [32] N. Devine, A. Ankiewicz, G. Genty, J. M. Dudley, and N. Akhmediev, Recurrence phase shift in Fermi-Pasta-Ulam nonlinear dynamics, *Phys. Lett. A* **375**, 4158 (2011).
- [33] G. Vanderhaegen, C. Naveau, P. Szriftgiser, A. Kudlinski, M. Conforti, A. Mussot, M. Onorato, S. Trillo, A. Chabchoub, and N. Akhmediev, “Extraordinary” modulation instability in optics and hydrodynamics, *Proc. Natl. Acad. Sci. USA* **118**, e2019348118 (2021).
- [34] M. Wu and C. E. Patton, Experimental Observation of Fermi-Pasta-Ulam Recurrence in a Nonlinear Feedback Ring System, *Phys. Rev. Lett.* **98**, 047202 (2007).
- [35] H. C. Yuen and W. E. Ferguson Jr., Relationship between Benjamin-Feir instability and recurrence in the nonlinear Schrödinger equation, *Phys. Fluids* **21**, 1275 (1978).
- [36] G. Van Simaey, P. Emplit, and M. Haelterman, Experimental study of the reversible behavior of modulational instability in optical fibers, *J. Opt. Soc. Am. B* **19**, 477 (2002).
- [37] N. J. Zabusky and M. D. Kruskal, Interaction of “Solitons” in a Collisionless Plasma and the Recurrence of Initial States, *Phys. Rev. Lett.* **15**, 240 (1965).
- [38] N. N. Akhmediev and A. Ankiewicz, *Nonlinear Pulses and Beams* (Springer, New York, 1997).
- [39] T. Dauxois and M. Peyrard, *Physics of Solitons* (Cambridge University Press, Cambridge, 2006).
- [40] C. S. Gardner, J. M. Greene, M. D. Kruskal, and R. M. Miura, Method for Solving the Korteweg-deVries Equation, *Phys. Rev. Lett.* **19**, 1095 (1967).
- [41] P. D. Lax, Integrals of nonlinear equations of evolution and solitary waves, *Commun. Pure Appl. Math.* **21**, 467 (1968).
- [42] N. Akhmediev and V. Korneev, Modulation instability and periodic solutions of the nonlinear Schrödinger equation, *Theor. Math. Phys.* **69**, 1089 (1986).
- [43] S. A. Chin, O. A. Ashour, and M. R. Belić, Anatomy of the Akhmediev breather: Cascading instability, first formation time, and Fermi-Pasta-Ulam recurrence, *Phys. Rev. E* **92**, 063202 (2015).
- [44] H. Yin and K. Chow, Breathers, cascading instabilities and Fermi-Pasta-Ulam-Tsingou recurrence of the derivative nonlinear Schrödinger equation: Effects of ‘self-steepening’ nonlinearity, *Physica D (Amsterdam)* **428**, 133033 (2021).
- [45] M. Conforti, A. Mussot, A. Kudlinski, S. Trillo, and N. Akhmediev, Doubly periodic solutions of the focusing nonlinear Schrödinger equation: Recurrence, period doubling, and amplification outside the conventional modulation-instability band, *Phys. Rev. A* **101**, 023843 (2020).
- [46] H. Yin, Q. Pan, and K. Chow, Four-wave mixing and coherently coupled Schrödinger equations: Cascading processes and Fermi-Pasta-Ulam-Tsingou recurrence, *Chaos* **31**, 083117 (2021).
- [47] G. Zhang, Z. Yan, and X.-Y. Wen, Three-wave resonant interactions: Multi-dark-dark-dark solitons, breathers, rogue waves, and their interactions and dynamics, *Physica D (Amsterdam)* **366**, 27 (2018).
- [48] S. Chen, F. Baronio, J. M. Soto-Crespo, P. Grelu, and D. Mihalache, Versatile rogue waves in scalar, vector, and multidimensional nonlinear systems, *J. Phys. A: Math. Theor.* **50**, 463001 (2017).
- [49] T. Yoshinaga, M. Wakamiya, and T. Kakutani, Recurrence and chaotic behavior resulting from nonlinear interaction between long and short waves, *Phys. Fluids A* **3**, 83 (1991).
- [50] A. Mussot, A. Kudlinski, M. Droques, P. Szriftgiser, and N. Akhmediev, Fermi-Pasta-Ulam Recurrence in Nonlinear Fiber Optics: The Role of Reversible and Irreversible Losses, *Phys. Rev. X* **4**, 011054 (2014).
- [51] J. P. Boyd, Theta functions, Gaussian series, and spatially periodic solutions of the Korteweg-de Vries equation, *J. Math. Phys.* **23**, 375 (1982).
- [52] T. Miloh, On periodic and solitary wavelike solutions of the intermediate long-wave equation, *J. Fluid Mech.* **211**, 617 (1990).
- [53] N. V. Priya, M. Senthilvelan, and M. Lakshmanan, Akhmediev breathers, Ma solitons, and general breathers from rogue waves: A case study in the Manakov system, *Phys. Rev. E* **88**, 022918 (2013).
- [54] L.-C. Zhao, G.-G. Xin, and Z.-Y. Yang, Rogue-wave pattern transition induced by relative frequency, *Phys. Rev. E* **90**, 022918 (2014).
- [55] J. M. Soto-Crespo, N. Devine, and N. Akhmediev, Integrable Turbulence and Rogue Waves: Breathers or Solitons? *Phys. Rev. Lett.* **116**, 103901 (2016).
- [56] P. Grinevich and P. Santini, The exact rogue wave recurrence in the NLS periodic setting via matched asymptotic expansions, for 1 and 2 unstable modes, *Phys. Lett. A* **382**, 973 (2018).
- [57] P. Grinevich and P. Santini, The finite gap method and the analytic description of the exact rogue wave recurrence in the periodic NLS Cauchy problem. 1, *Nonlinearity* **31**, 5258 (2018).
- [58] A. Chabchoub, N. Hoffmann, E. Tobisch, T. Waseda, and N. Akhmediev, Drifting breathers and Fermi-Pasta-Ulam paradox for water waves, *Wave Motion* **90**, 168 (2019).
- [59] J. Zheng, G. Wang, G. Dong, X. Ma, and Y. Ma, Numerical study on Fermi-Pasta-Ulam-Tsingou problem for 1D shallow-water waves, *Wave Motion* **51**, 157 (2014).